RSC Advances

PAPER

View Article Online
View Journal | View Issue

Cite this: *RSC Adv.*, 2023, **13**, 15391

A pyridine dicarboxylate based hydrazone Schiff base for reversible colorimetric recognition of Ni^{2+} and PPi†

Rashim Bawa,[a] Swati Negi,[a] Bholey Singh,[b] Balaram Pani[c] and Rakesh Kumar*[a]

A pyridine dicarboxylate Schiff-base **DAS** was synthesized for cascade colorimetric recognition of Ni^{2+} and PPi. The selectivity and sensitivity of chemosensor **DAS** was investigated through colorimetric and UV-vis studies in MeOH-PBS (5 : 1, v/v, pH = 7.4). The chemosensor formed a 2 : 1 complex with Ni^{2+} metal ions with a binding constant of $K_a = 3.07 \times 10^3\ M^{-2}$. Besides, a plausible sensing mechanism is confirmed by single crystal X-ray diffraction (SC-XRD), Job's plot and Benesi–Hildebrand plot (B–H plot) experiments. Furthermore, the **DAS**-Ni^{2+} ensemble formed *'in situ'* was used to selectively recognise PPi. The limit of detection (LOD) of **DAS** for Ni^{2+} was found to be 0.14 μM and that of the **DAS**-Ni^{2+} ensemble for PPi was found to be 0.33 μM. Also, the potential of the chemosensor has been applied for solid state detection of Ni^{2+} as well as to mimic the 'INHIBIT' logic gate on the addition of Ni^{2+} ions and PPi.

Received 28th March 2023
Accepted 12th May 2023

DOI: 10.1039/d3ra02021e

rsc.li/rsc-advances

1. Introduction

Among the various transition metals, Ni^{2+} is a vitally important trace metal which is involved in various industrial processes such as electroplating, the production of rechargeable batteries, catalysts in chemical reactions and electronic equipment. The nickel composites especially stainless steel, are used in different tools and appliances. Due to its toxic nature, Ni^{2+} compounds have been classified as carcinogenic to humans in group I by the International Agency for Research on Cancer.[1] The vast usage of Ni^{2+} in industries impacts human health and also leads to environmental pollution. Apart from this, Ni^{2+} also plays a vital role as an essential micronutrient in plants and animals. However, its overexposure may cause serious ailments such as asthma, central nervous system disorders, kidney diseases, lung fibrosis and cancer.[2] Therefore, selective monitoring of Ni^{2+} through effective methods has become an obligatory task for clinical as well as environmental analysis.[3]

Different strategies have been reported for the recognition and quantification of Ni^{2+} in environment as well as biology. The majority of chemosensors are centered on potentiometric techniques,[4] atomic absorption spectroscopy[5] and liquid chromatography.[6] However these methods show more time consumption, tedious sample preparation and high maintenance.[7] Even though these methods show accuracy, they show inconvenience for field analysis. Alternatively, fluorescence and colorimetric chemosensors provide easy sample preparation, high sensitivity and selectivity and are also cost effective.[8,9] As compared to fluorescent chemosensors which require UV-vis as well as fluorescence spectrophotometer,[10–12] colorimetric chemosensors require only UV-vis spectrophotometric. Additionally, colorimetric chemosensors are most convenient as they provide naked-eye detection of the analyte *via* colour changes. Although, many researchers have focused on the evolution of fluorescent and colorimetric chemosensors for Ni^{2+}; however most of them show interference with other metal ions.[13,14] There are very few reports for the selective recognition of Ni^{2+} that have been published in literature.[15–18] A number of Schiff bases as colorimetric sensors have been reported for the recognition of different analytes of biological and environmental importance.[19,20] The importance of anionic species in biology, environment and medicine has increased the interest of researchers in developing organic chemo sensors for their recognition.[21–23] Among different anions, pyrophosphate (PPi or $P_2O_7^{4-}$) plays an elemental role in biological processes as it is a product of ATP hydrolysis under cellular conditions.[24] PPi is involved in certain processes such as protein synthesis, gene transcription and cellular signal transduction.[25] The concentration of PPi provides critical information on processes such as DNA replication and DNA sequencing.[26] The alterations in the content of PPi may lead to different diseases.[27] In recent years, the recognition of PPi has become crucial in cancer research.[28] One of the most successful strategies for the designing chemosensors for PPi is

[a]*Bioorganic Laboratory, Department of Chemistry, University of Delhi, Delhi, 110007, India. E-mail: rakeshkp@email.com*

[b]*Department of Chemistry, Swami Shraddhanand College, University of Delhi, Delhi 110036, India*

[c]*Department of Chemistry, Bhaskaracharya College of Applied Sciences, University of Delhi, Delhi 110075, India*

† Electronic supplementary information (ESI) available. CCDC 2206485 and 2206486. For ESI and crystallographic data in CIF or other electronic format see DOI: https://doi.org/10.1039/d3ra02021e

the incorporation of metal-complexes in the system. This is because of the fact that there is a strong binding between the metal ion and PPi allowing the recognition of PPi.[29] In these "metal-containing chemosensing ensembles" different transition metal ions such as copper,[30] zinc,[31,32] aluminium[33] and ferric[34,35] have been used in literature for the recognition of PPi. However, so far, to our knowledge, such systems with nickel to detect PPi, have not been reported in literature. Nowadays, chemosensors have been interestingly used in the fields of molecular logic gates, information storage devices and molecular keypad locks. They play an important role in molecular computers by translating chemically ciphered information (input) to optical signals (output). The cascade recognition ability of **DAS** has facilitated its use in molecular logic gates based on its colorimetric response.

Herein, we have synthesized a novel pyridine-dicarboxylate based hydrazone Schiff base **DAS** using simple convenient routes, which acted as a potential colorimetric chemosensor for selective recognition of Ni^{2+} and PPi *via* "naked-eye" colour changes.

2. Experimental

2.1. Materials and methods

Ethyl acetoacetate, 2-hydroxybenzohydrazide and selenium dioxide were obtained from Spectrochem Pvt. Ltd and were used without any further purifications. For the purpose of synthesis and photophysical studies some reagents, metal salts and phosphates were acquired from Sigma-Aldrich and Sisco Research Laboratories. The solvents used for absorption studies were of HPLC grade. The stock solutions of metal salts and phosphates were prepared in double distilled water. The melting point of compounds were recorded on Buchi M-560 melting point apparatus. ^{1}H NMR and ^{13}C NMR spectra were obtained on a JNM-EXCP 400 (JEOL, USA) spectrometer operating at 400 and 100 MHz, respectively. The FT-IR spectra were obtained on PerkinElmer 2000 Fourier Transform Infrared spectrometer. A 1 cm quartz cuvette was used on Carey Series UV-vis spectrophotometer to record the absorption data.

2.1.1. Synthesis of diethyl 2-formyl-6-methyl-4-(4-nitrophenyl)pyridine-3,5-dicarboxylate (2). Diethyl 2,6-dimethyl-4-(4-nitrophenyl)-1,4-dihydropyridine-3,5-dicarboxylate (**1**, 1 g, 1 mmol) was added to a solution of selenium dioxide (740 mg, 2.5 mmol) in 1,4-dioxane. The reaction mixture was refluxed and the reaction was monitored by TLC (Scheme 1). The reaction completed within 10 min. After the completion of reaction, the reaction mixture was cooled at room temperature and then filtered to remove selenium. The obtained filtrate was then evaporated under reduced pressure to procure the crude mixture of two compounds **2** and **3** separated by column chromatography (hexane: ethyl acetate, 7 : 3, v/v) in 59% and 41% yield. The structure of compound **2** was further confirmed by ^{1}H, ^{13}C NMR, IR and HRMS analysis.

^{1}H NMR (400 MHz, DMSO-d_6): δ ppm 9.95 (s, 1H), 8.30 (d, J = 8.8 Hz, 2H), 7.47 (d, J = 8.8 Hz, 2H), 4.01 (m, J = 7.1, 2.2 Hz, 4H), 2.63 (s, 3H), 0.92 (t, J = 7.1 Hz, 3H), 0.85 (t, J = 7.1 Hz, 3H). ^{13}C NMR (100 MHz, DMSO-d_6): δ ppm 192.7, 166.0, 165.4, 157.2, 147.6, 144.7, 140.7, 130.4, 123.5, 62.5, 62.2, 22.5, 13.5. IR (KBr, cm^{-1}): 2895, 2860 and 1720. Melting point: 130–132 °C. HRMS (m/z): Calculated for $C_{19}H_{18}N_2O_7$ 387.1148, obtained 387.1187.

2.1.2. Synthesis of diethyl (*E*)-2-((2-(2-hydroxybenzoyl) hydrazono)methyl)-6-methyl-4-(4-nitrophenyl)pyridine-3,5-dicarboxylate (DAS). An ethanolic solution of 2-hydroxybenzohydrazide (**4**, 200 mg, 1 mmol) was prepared in the presence of acetic acid (1 mL). Diethyl 2-formyl-6-methyl-4-(4-nitrophenyl) pyridine-3, 5-dicarboxylate (**2**, 500 mg, 1 mmol) was added to this mixture and further refluxed. The progress of product formation was monitored using TLC and all the reactants were consumed within 6 hours (Scheme 2). Further, the reaction mixture was cool down to room temperature and a white precipitates was observed at the bottom of the flask. The precipitates were filtered and washed several times with cold ethanol to obtain pure white crystalline solid in 89% yield. The compound **DAS** was confirmed by ^{1}H, ^{13}C NMR, IR and HRMS analysis.

^{1}H NMR (400 MHz, DMSO-d_6): δ ppm 12.03 (s, 1H), 11.41 (s, 1H), 8.45 (s, 1H), 8.30 (d, J = 8.5 Hz, 2H), 7.77 (s, 1H), 7.49 (s, 2H), 7.43–7.37 (s, 1H), 6.96–6.92 (m, 2H), 4.11 (q, J = 7.0 Hz, 2H), 3.98 (q, J = 7.1 Hz, 2H), 2.57 (s, 3H), 0.91 (t, J = 7.0 Hz, 3H), 0.84 (t, J = 7.1 Hz, 3H).

^{13}C NMR (100 MHz, DMSO-d_6): δ ppm 166.4, 156.0, 149.6, 148.1, 144.5, 141.9, 130.3, 129.5, 128.2, 123.7, 119.5, 117.6, 62.1, 23.0, 13.8. IR (KBr, cm^{-1}): 3320, 2976, 1726, 1601 and 1210. Melting point: 147–149 °C. HRMS (m/z): Calculated for $C_{26}H_{24}N_4O_8$ 521.1628, obtained 521.1621.

2.1.3. Preparation of samples and UV-vis studies. The stock solutions of chlorides and nitrates (10 mM) of metal ions (Ni^{2+}, Cu^{2+}, Fe^{2+}, Fe^{3+}, Cr^{3+}, Hg^{2+}, Mn^{2+}, Pb^{2+}, Ag^+ and Cd^{2+}), sodium salts (10 mM) of phosphates (PPi, $H_2PO_4^-$, HPO_4^-, AMP, ADP and ATP) were prepared in double distilled water. The stock solution of chemosensor **DAS** (1 mM) was prepared in MeOH-PBS (5 : 1, v/v, pH = 7.4). The metal and phosphate binding studies were carried out by adding 6 μL of stock solutions of metal ions or phosphates to 20 μM solution in 2.94 mL solution **DAS** or **DAS**-Ni^{2+} ensemble, respectively, in MeOH-PBS (5 : 1, v/v, pH = 7.4). The competitive binding studies were performed by adding 3 μL of Ni^{2+} or PPi to 2.94 mL of **DAS** or **DAS**-Ni^{2+} ensemble, respectively, in cuvette, followed by the addition of 3 μL of other metal ion or phosphate solutions.

2.1.4. Calculation of binding constants, binding stoichiometry & detection limit. The absorption titration experiments were carried out to calculate the binding affinity of **DAS** with Ni^{2+} by sequential addition of Ni^{2+} (0–20 μM). Further, the absorption spectra was used to make Benesi–Hildebrand Plot of $1/[Ni^{2+}]$ *vs.* $1/(A - A_0)$. The binding constant (K_a) for the formation of the complex with Ni^{2+} was examined from the B–H plot using following eqn (1).[36]

$$\frac{1}{(A - A_0)} = \frac{1}{K_a(A_{max} - A_0)C} + \frac{1}{(A_{max} - A_0)} \quad (1)$$

Here and A and A_0 are the maximum absorption intensities of the **DAS** in the presence and absence of Ni^{2+} ion, respectively. C is the concentration of Ni^{2+} ion added while the titration

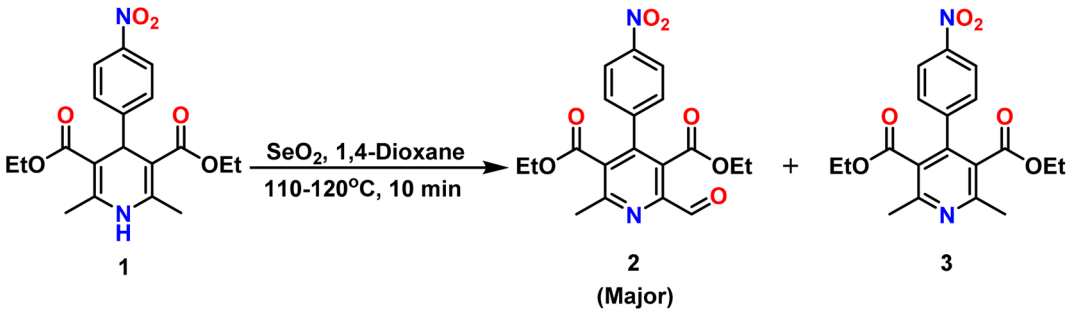

Scheme 1 Synthesis of compound 2.

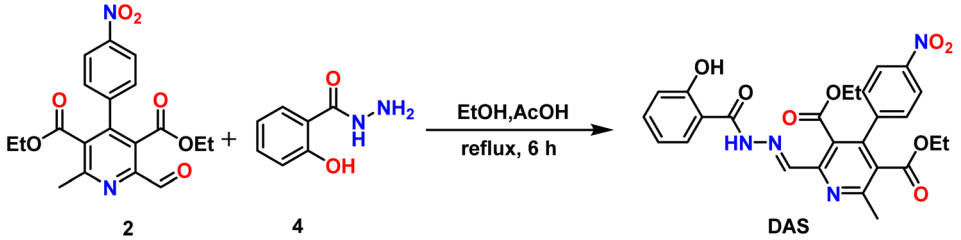

Scheme 2 Synthetic route to DAS.

experiment, K_a is known as binding constant and A_{max} stands for maximum absorption intensity which was noticed after successive addition of Ni^{2+} ion.

In order to obtain the binding stoichiometry, stock solutions of **DAS** and Ni^{2+} with concentration 20 μM were prepared in MeOH-PBS (5 : 1 v/v, 10 mM, pH = 7.4) and deionized water, respectively. Further, titrations were carried out by adding 0.3–3 mL of **DAS** and 3–0.3 mL of Ni^{2+} ion in the quartz cuvette to make the final volume to 3 mL and recorded the absorption spectra of the solution. A graph was plotted between mole fraction of $Ni^{2+}(X_{Ni}{}^{2+})$ and $(A_0 - A) \times X_{Ni}{}^{2+}$ to obtain job's plot.[37]

The limit of detection (LOD) of **DAS** for Ni^{2+} was evaluated by using following eqn (2).[38]

$$\mathrm{LOD} = \frac{3\sigma}{K_a} \quad (2)$$

The standard deviation (σ) was calculated by taking ten replicate absorption measurements while binding constant K_a was calculated from the slope of B–H plot.

3. Results and discussion

3.1. Synthesis

The chemosensor **DAS** was synthesized by mixing ethanolic solutions of diethyl 2-formyl-6-methyl-4-(4-nitrophenyl) pyridine-3,5-dicarboxylate (**2**) and 2-hydroxybenzohydrazide (**4**) and then added a 1 mL of acetic acid to the reaction mixture. After the addition, reaction mixture was refluxed for 6 hours to obtain final product **DAS** in 89% yield. The synthesis of compound **2**, precursor of the final compound, that was obtained by the oxidation of diethyl 2,6-dimethyl-4-(4-nitrophenyl)-1,4-dihydropyridine-3,5-dicarboxylate (**1**) using the oxidizing agent SeO_2 in 1,4-dioxane. The oxidation lead to the formation of two products *i.e.* diethyl 2-formyl-6-methyl-4-(4-nitrophenyl) pyridine-3,5-dicarboxylate (**2**, major) and diethyl 2,6-dimethyl-4-(4-nitrophenyl) pyridine-3,5-dicarboxylate (**3**, minor) (Scheme 1) which were separated by column chromatography. All the synthesized compounds were confirmed by ^1H, ^{13}C NMR, IR and HRMS Data.

3.2. Colorimetric detection of Ni^{2+}

The colorimetric sensing of the ligand **DAS** was carried out by addition of various metal ions to solution of **DAS** in MeOH-PBS (5 : 1 v/v, 10 mM, pH = 7.4). Only on the addition of Ni^{2+}, an instant eye-catching change from colorless to yellow was observed and on addition of other metal ions there is no visible color changes were observed (Fig. 1).

3.3. UV-vis studies

The UV-vis titration studies was performed to get insight about the sensing ability of chemosensor **DAS** towards various metal ions. The UV-vis absorption spectrum of **DAS** (20 μM) were recorded in MeOH-PBS (5 : 1 v/v, 10 mM, pH = 7.4) which unveiled a broad band at 320 nm (Fig. 2a). which might be attributed to the π–π* or n–π* charge transfer within the ligand. The cation sensing of chemosensor **DAS** was carried out by addition of 1 equiv. salts of metal ions into stock solution of **DAS**, no notable changes were perceived in its absorption spectra. However, on addition of Ni^{2+} to the solution of **DAS**, a new prominent band was observed in the following spectra as shown in (Fig. 2b). It could be seen in (Fig. 2c) that in the presence of Ni^{2+}, the intensity of the CT band of **DAS** that was

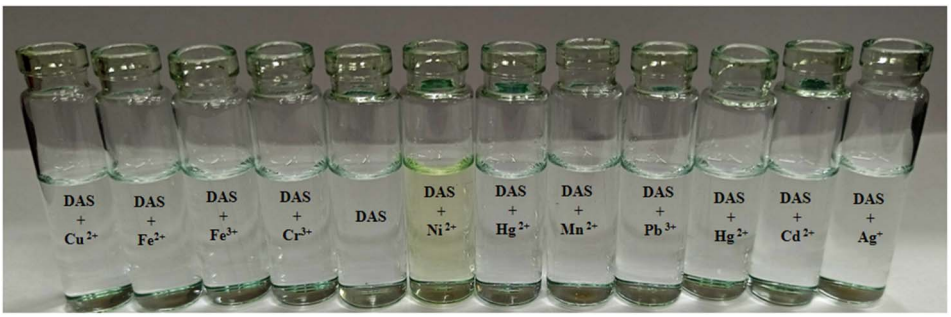

Fig. 1 The visible changes in color of **DAS** (20 μM) after addition of 1 equiv. of various metal salts.

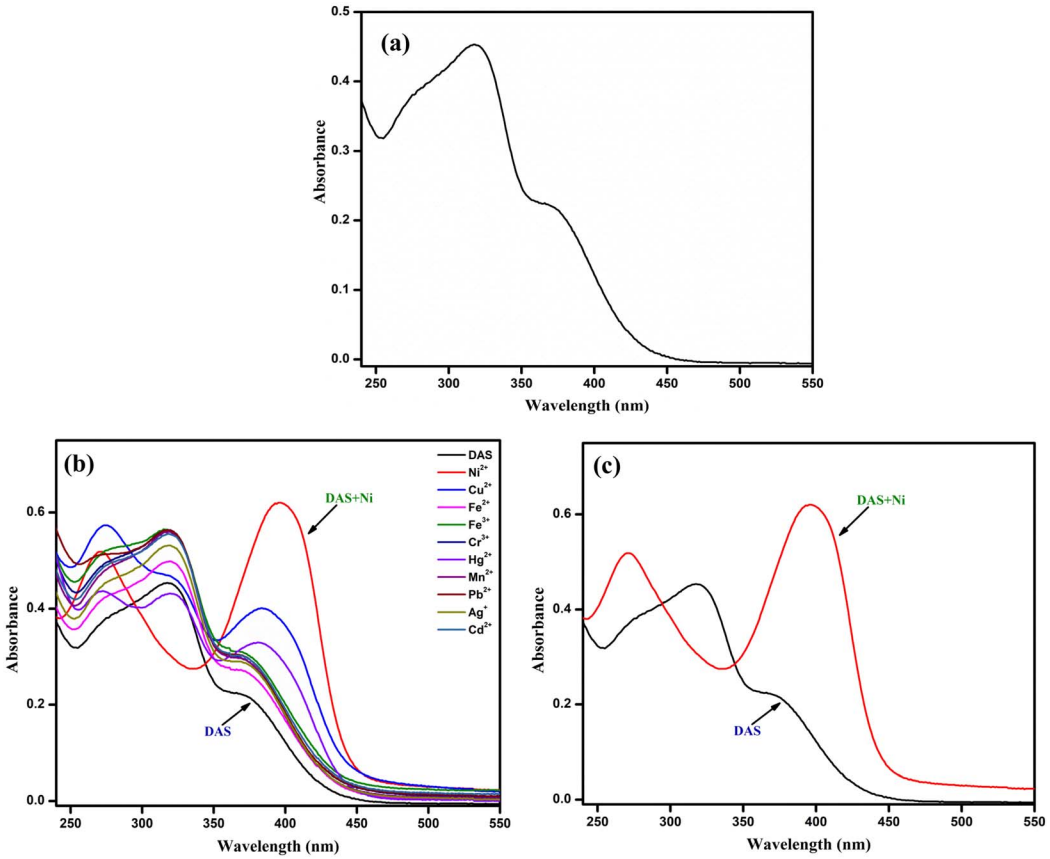

Fig. 2 (a) The absorption spectrum of **DAS** (20 μM). (b) UV-vis Spectral changes of **DAS** on addition of 1 equiv. of various metal ions. (c) Absorption spectra of **DAS** and **DAS**-Ni^{2+}.

centered at 320 nm disappeared and new bands at 270 and 400 nm appeared. The isobestic points at 290 and 345 nm suggested the formation of a stable complex between Ni^{2+} and **DAS**.

3.4. Selectivity study

It is imperative to examine the selectivity of chemosensor because having high selectivity is one of the essential requirement of good chemosensor. Therefore, to evaluate the selectivity of **DAS**, interference experiment was carried out by adding different metal ions into the solution of Ni^{2+} ion (Fig. 3). A similar patterns was observed in the absorption studies of **DAS** having Ni^{2+} in the presence of other metal ions which indicated that recognition of Ni^{2+} ion is not affected by other coexisting metal ions. On the basis of response towards the intervening samples, the chemosensor, **DAS** showed high selectivity for Ni^{2+} even in the presence of other metals under same conditions.

3.5. Binding stoichiometry analysis of DAS towards Ni^{2+}

To understand more about the interaction between **DAS** and Ni^{2+}, titration studies were performed in MeOH-PBS (5 : 1 v/v, 10 mM, pH = 7.4). It could be observed that on sequential

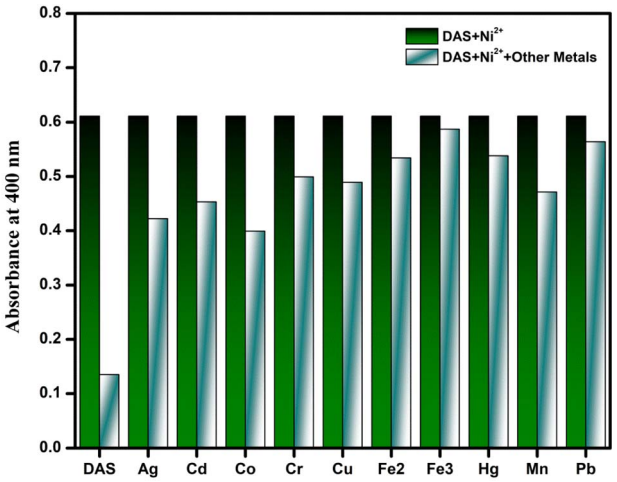

Fig. 3 Absorbance data for DAS-Ni^{2+} in the existence of 1 equiv. of different metal ions.

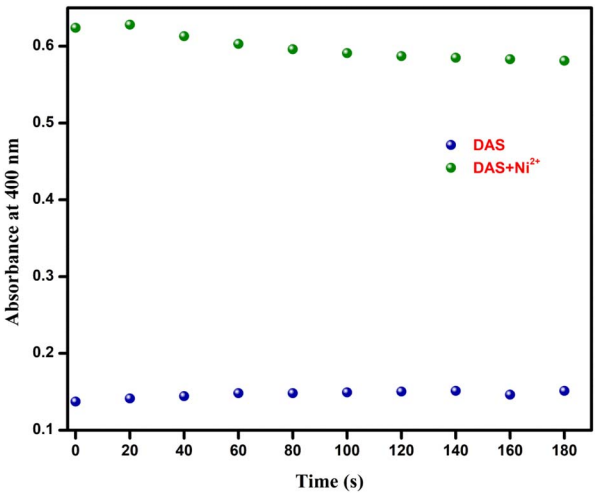

Fig. 5 Absorption response of DAS (20 μM, MeOH-PBS, pH = 7.4, 5 : 1, v/v) at the wavelength 400 nm in the presence of Ni^{2+} (1 equiv.) with respect to time.

addition of Ni^{2+} to the solution of **DAS** the absorption peak at 320 nm disappeared while the intensity of new peaks at 270 nm and 400 nm gradually increased (Fig. 4a). Furthermore, the binding constant (K_a) and binding stoichiometry for complex formation were determined by applying B–H and Job's plot, respectively. The Job's plot (Fig. 4b); revealed that the maximum was achieved when the molar ratio of the **DAS** and Ni^{2+} were at 0.4. This indicated 2 : 1 binding stoichiometry between **DAS** and Ni^{2+}.

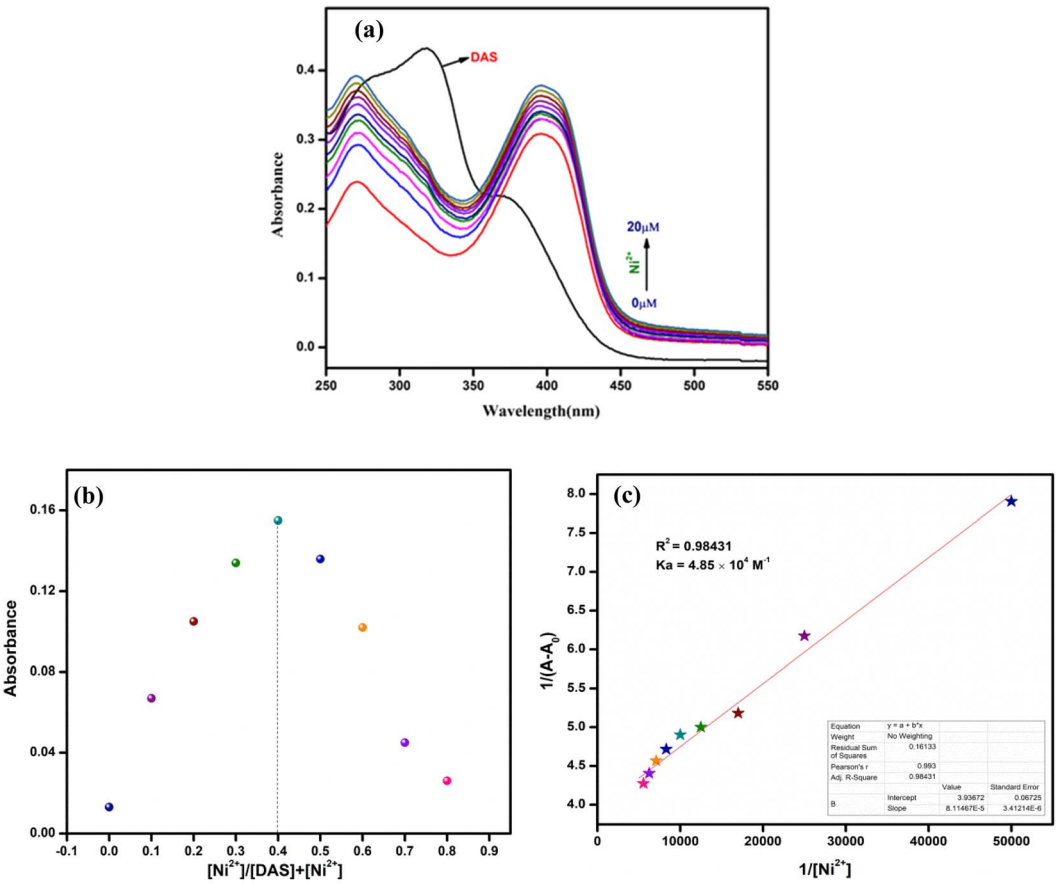

Fig. 4 (a) Absorption spectra of **DAS** (20 μM) on sequential addition of Ni^{2+} (0–20 μM). (b) Job's Plot for UV-vis studies of **DAS** with Ni^{2+} in MeOH-PBS (5 : 1 v/v, 10 mM, pH = 7.4). (c) B–H Plot for UV-vis studies of **DAS** with Ni^{2+} in MeOH-PBS (5 : 1, v/v, 10 mM, pH = 7.4).

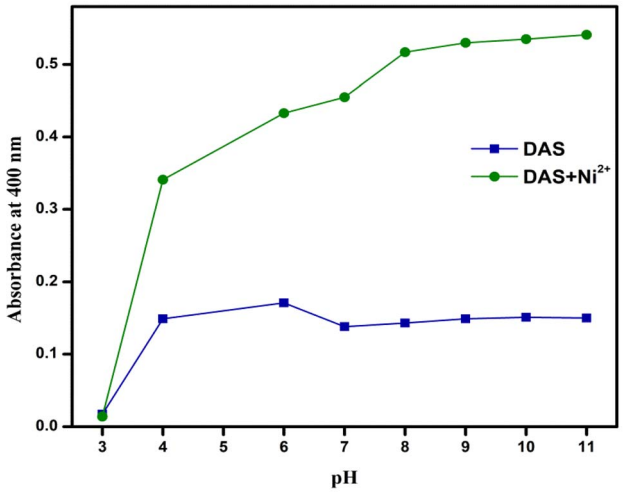

Fig. 6 The Effect of pH on the absorption intensity of DAS at 400 nm.

The B–H plot of $1/[Ni^{2+}]$ *vs.* $1/[A - A_0]$ showed linearity with $R^2 = 0.98448$, which also confirmed 2 : 1 binding stoichiometry of the complex (Fig. 4c). The binding/association constant of **DAS** for Ni^{2+} was found out to be 3.07×10^3 M^{-2}.

3.6. Limit of detection & time response

The limit of detection of chemosensor **DAS** was calculated to be 0.14 μM, implicating that the chemosensor could be used for colorimetric recognition of Ni^{2+} even at lower concentrations. When 1 equiv. of Ni^{2+} was added into the solution of **DAS**, the absorbance of **DAS** at 400 nm changed and remained constant afterwards (Fig. 5). The swift sensing of **DAS** made it appropriate for real time detection of Ni^{2+}.

3.7. Effect of pH

The colorimetric response of **DAS** in the absence and presence of Ni^{2+} was studied as a function of pH. The pH was adjusted by the addition of 1 M hydrochloric acid (HCl) and sodium hydroxide (NaOH) solutions. As seen in the figure, no detection of Ni^{2+} observed at pH = 3, probably due to protonation of **DAS**.

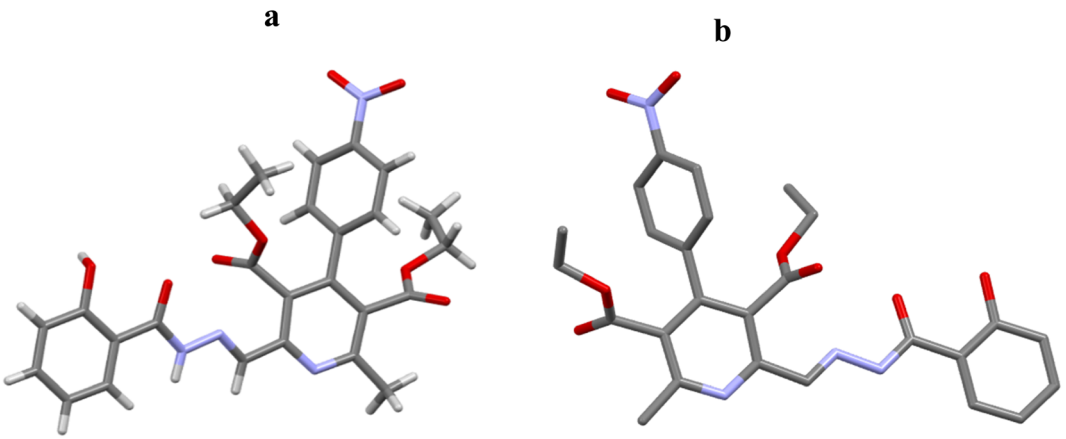

Fig. 7 Molecular structures (a) and (b) of DAS. For clarity hydrogen atoms are omitted in structure b. gray = C, blue = N, red = O.

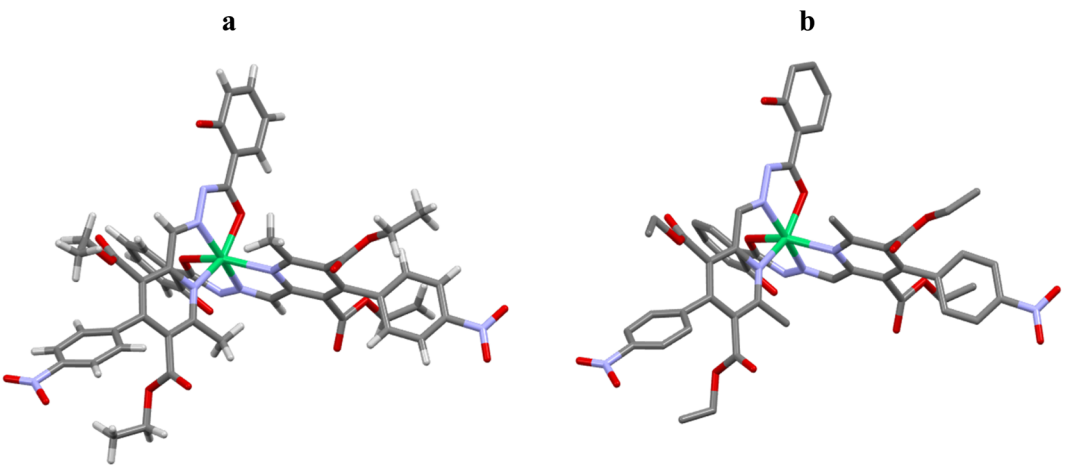

Fig. 8 Molecular structures (a) and (b) of DAS-Ni^{2+}. For clarity hydrogen atoms are omitted in structure b. green = Ni, gray = C, blue = N, red = O.

Table 1 Some important bond angles and bond lengths with Ni^{2+} metal ion to adjacent atoms

Atom(s)	Bond angle (°)	Atom(s)	Bond length (Å)
∠N17–Ni2–O33	77.8(4)	Ni2–N20	2.17
∠N17–Ni2–O42	89.2(4)	Ni2–N15	2.20
∠N20–Ni2–N21	77.2(4)	Ni2–N17	1.97
∠N20–Ni2–O33	89.4(3)	Ni2–N21	1.98
∠N20–Ni2–O42	154.7(4)	Ni2–O33	2.067
∠N21–Ni2–O33	95.0(4)	Ni2–O42	2.077
∠N21–Ni2–O42	77.6(4)		
∠O33–Ni2–O42	90.5(3)		

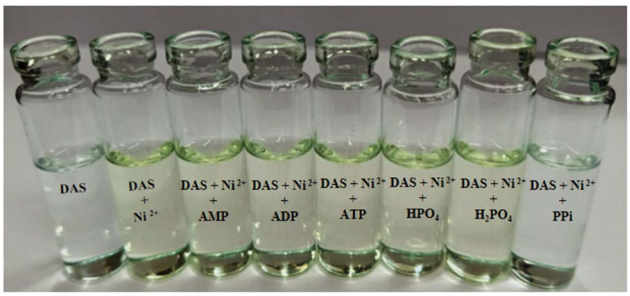

Fig. 9 Colorimetric changes observed in DAS-Ni^{2+} (20 μM) upon addition of 1 equiv. of different phosphates.

As the pH increased, the sensing ability of **DAS** for Ni^{2+} increased and then became almost constant after pH = 8. Therefore, it could be inferred that the chemosensor was suitable for detection of Ni^{2+} under conditions of physiological pH (Fig. 6).

3.8. SC-XRD analysis of DAS and DAS-Ni^{2+}

Single crystal structures of compound **DAS** and metal complex **DAS**-Ni^{2+} were determined by SC-XRD studies which disclosed that crystal structure of metal complex include Ni^{2+} atom coordinated with two nitrogen and one oxygen atom supported by aromatic ring in the ratio 2 : 1 and also confirmed through the Job's plot method while in the compound these atoms are free which is clearly shown in (Fig. 7). In the metal complex, pyridine ring and another N∩O chelating moiety binds to the metal in a square planar geometry which is confirmed by the bond angles analysis (∠N17–Ni2–O33, O42 are 77.8(4), 89.2(4) & N20–Ni2–N21, O33, O42 are 77.2(4), 89.4(3) and 154.7(4) and N21–Ni2–O33, O42 are 95.0(4), 77.6(4) and O33–Ni2–O42 is 90.5(3) respectively (Fig. 8). The Ni atom is bridged *via* N and O atoms offering (N∩O) bis-chelating units and display conventional structural parameters. The Ni2–N20, N15 bond distances lie in 2.17–2.20 Å and Ni2–N17, N21 in 1.97–1.98 Å range whereas Ni2–O33 bond length lie close to that of Ni2–O42 (2.067–2.077 Å). These findings support that nickel ion coordinated with [N\O] bis-chelating units (Table 1).

3.9. Phosphate sensing by DAS-Ni^{2+} ensemble

Sodium salts of different phosphate such as AMP, ADP, ATP, HPO_4, H_2PO_4 and PPi were added to solution of **DAS**-Ni^{2+} in MeOH-PBS (5 : 1, v/v, 10 mM, pH = 7.4). Addition of PPi salt lead to immediate bleaching of the solution as the color of **DAS** (Fig. 9) and a notable change in the absorption spectra of **DAS**-Ni^{2+} (Fig. 10). However, no such variations were noticed after the addition of other phosphates.

It could be perceived in (Fig. 11) that in the existence of PPi, the intensity of the CT band of **DAS**-Ni^{2+} that was centered at 270 and 400 nm prominently disappeared and a new band at 320 nm appeared. This absorption spectrum obtained was the same as that of **DAS** in the absence of Ni^{2+}. The results also suggested the reversibility and reproducibility of the chemosensor using PPi by the following mechanism (Scheme 3).

To evaluate the selectivity of **DAS**-Ni^{2+} towards PPi over other phosphates, competitive binding studies were performed in the same solvent system. It was observed that no considerable

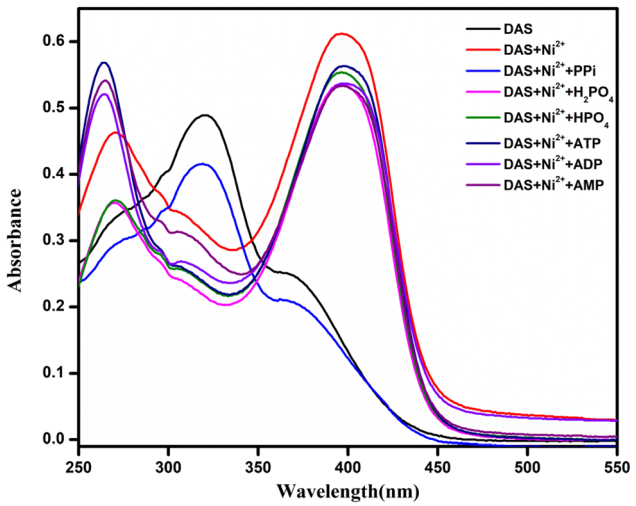

Fig. 10 UV-vis absorbance spectral changes in DAS-Ni^{2+} with addition of 1 equiv. of different phosphates.

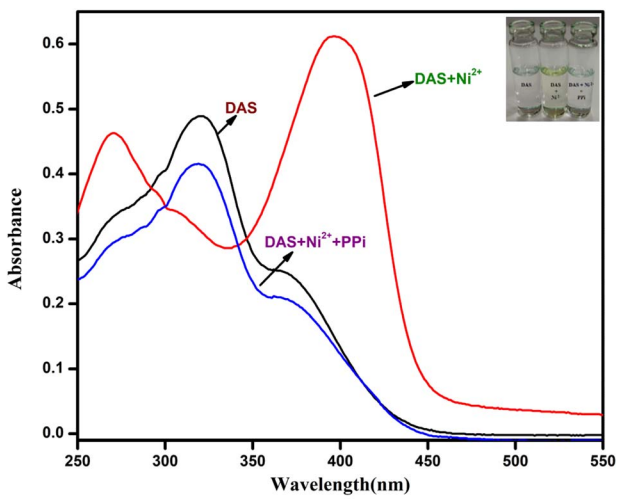

Fig. 11 Absorption spectra of DAS in the presence of Ni^{2+} and Ni^{2+} + PPi.

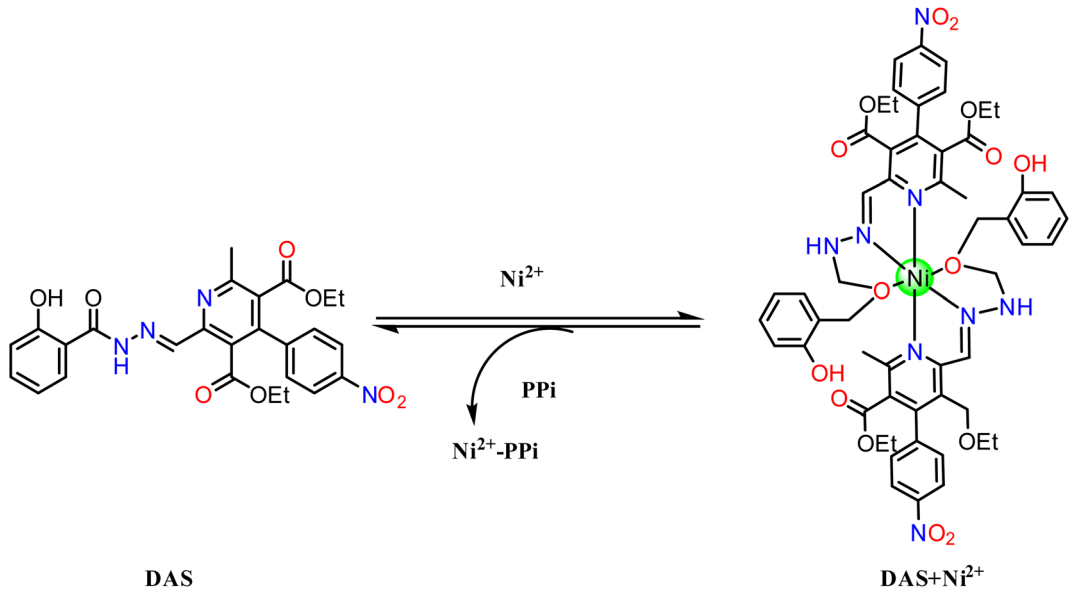

Scheme 3 Reversible binding of DAS with Ni^{2+} and PPi.

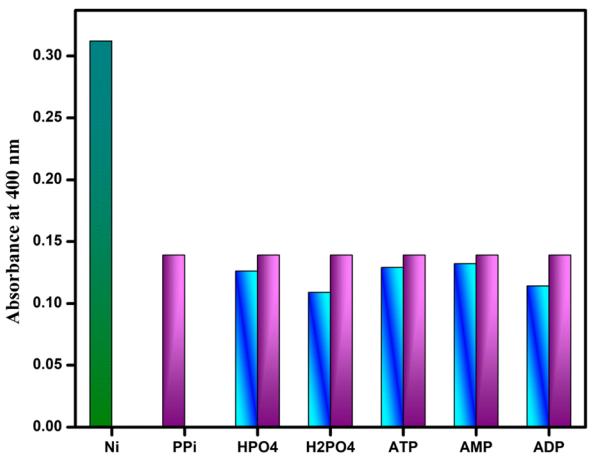

Fig. 12 Absorbance intensity of DAS-Ni^{2+} ensemble and PPi in the presence of other competitive phosphates.

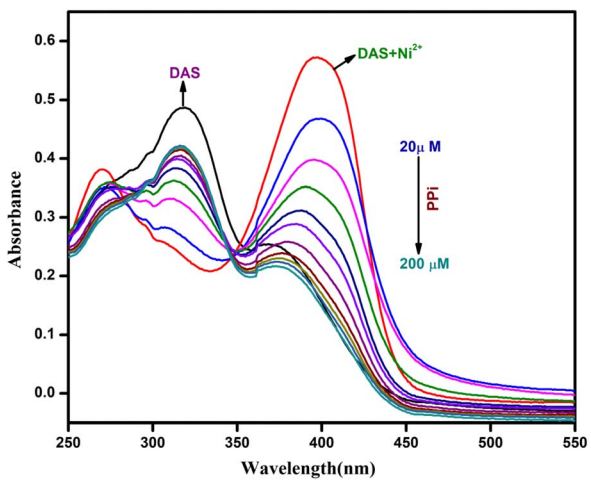

Fig. 13 Absorption spectra of DAS-Ni^{2+} ensemble on subsequent addition of PPi.

changes in the absorbance intensity at 400 nm were observed on the addition of other phosphates, as shown in (Fig. 12).

Further, we also calculated the binding constant (K_a) and the limit of detection of DAS-Ni^{2+} ensemble with PPi. It could be seen in (Fig. 13) that the successive addition of PPi to DAS-Ni^{2+} ensemble leads to a subsequent decrease and eventually the disappearance of bands at 270 and 400 nm. In addition to this, the absorption intensity at 320 nm started to increase.

The B–H plot obtained by plotting graph between 1/[PPi] *vs.* $1/(A - A_0)$ procured the value to binding constant to be $8.86 \times 10^3\ M^{-1}$ (Fig. 14).

The detection limit (Fig. 15) suggested that the ensemble had the ability to sense PPi even in concentrations as much as 0.33 μM. This detection limit was even better than that of other chemosensors reported for PPi.[39]

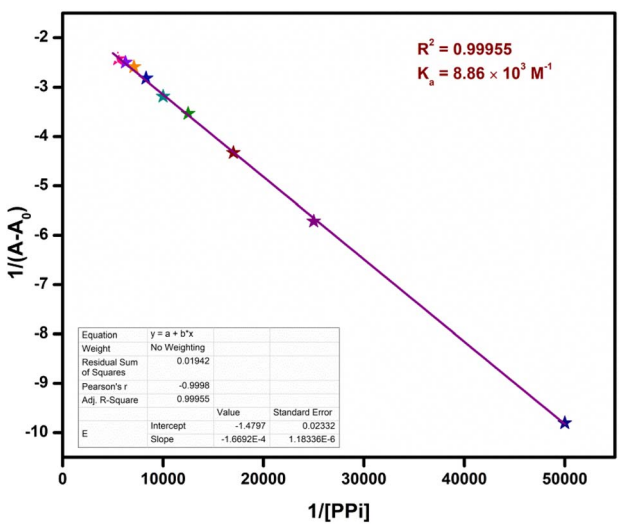

Fig. 14 B–H Plot of DAS-Ni^{2+} ensemble with PPi in MeOH-PBS (5 : 1 v/v, 10 mM, pH = 7.4).

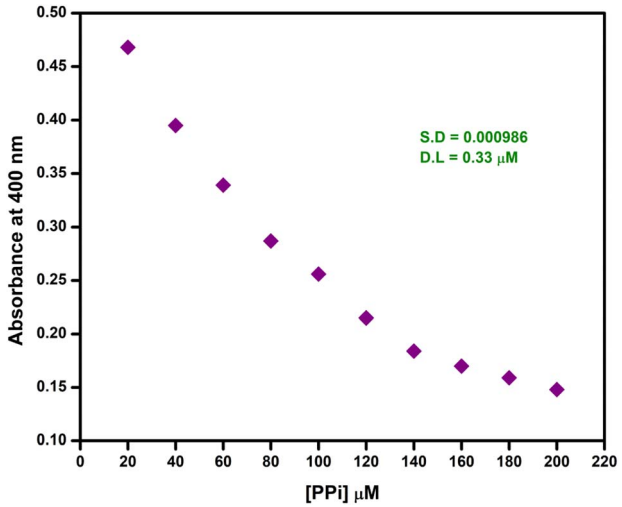

Fig. 15 Detection Limit of DAS-Ni^{2+} ensemble for PPi.

Fig. 16 Colorimetric reaction of DAS (50 μM in MeOH) towards Ni^{2+} in solid state.

3.10. Practical application of DAS

3.10.1. Solid state detection of Ni^{2+} by DAS. Silica gel (60–100 mesh size, 250 mg) was added to 50 μM solution of **DAS** in MeOH (2 mL). Further, the solvent was evaporated by vacuum distillation to acquire colorless silica. Similarly, silica gel was added to 50 μM solutions of **DAS** in MeOH containing 50 μM of Ni^{2+} salt. The solvent then evaporated under reduced pressure to afford yellow silica. The colorimetric response of **DAS** towards Ni^{2+} in solid state is shown in (Fig. 16).

3.10.2. Molecular logic gate property of DAS. The inputs are assigned as IN1 and IN2 for Ni^{2+} and PPi, respectively and the output as A_{400}. A truth table is created using binary digits as inputs, wherein, the presence and absence of Ni^{2+} and PPi was defined as "1" and "0", respectively.[40] When there is no chemical input, there is no absorbance at 400 nm *i.e.* when IN 1 = 0 and IN 2 = 0 then output = 0. However, when IN 1 = 1 and IN 2 = 0, the output = 1 as an absorption band is present at 400 nm in (Fig. 17).

4. Conclusions

In conclusion, a novel pyridine-dicarboxylate based hydrazone Schiff base (**DAS**) has been successfully synthesized which acted as a colorimetric chemosensor for recognition of Ni^{2+} ion and characterized *via* spectroscopic techniques. **DAS** exhibit fast and selective detection of Ni^{2+} even in the presence of other coexisting metal ions. Ni^{2+} formed 2 : 1 complex with **DAS** with binding constant $K_a = 3.07 \times 10^3\ M^{-2}$, as apparent from Job's plot and Benesi–Hildebrand plot (B–H plot). Besides, single crystal X-ray diffraction (SC-XRD) also validated the formation of a 2 : 1 complex between **DAS** and Ni^{2+}. The detection limit of **DAS** for Ni^{2+} has been found out to be 0.14 μM. **DAS**-Ni^{2+} ensemble formed "*in situ*" was found to show selective detection towards PPi with binding constant $K_a = 8.86 \times 10^3\ M^{-1}$ and detection limit of 0.33 μM. Moreover, **DAS** was demonstrated to mimic 'INHIBIT' logic gate on addition of Ni^{2+} and PPi. The chemosensor also showed a potential to detect Ni^{2+} in solid state. Since, colorimetric sensors for cascade sensing of Ni^{2+} and PPi have not been reported so far, **DAS** could be proved as a significant addition to the chemosensors earlier reported for Ni^{2+} or PPi.

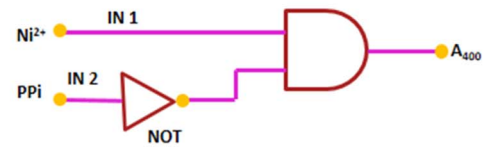

Ni^{2+} (IN 1)	PPi (IN 2)	A_{400}
0	0	0
1	0	1
0	1	0
1	1	0

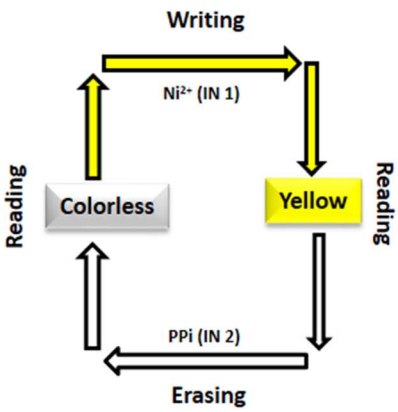

Fig. 17 'INHIBIT' logic gate depicting conditions mentioned in the truth table and schematic representation of logic gate operations for the memory element 'write-read-erase-read' functions.

Conflicts of interest

The authors have no conflict of interest to declare.

Acknowledgements

The authors R. B, S. N and R. K thanks to Council of Scientific & Industrial Research (CSIR), University Grants Commission (UGC) and Institute of Eminence (IoE), University of Delhi for financial support and University Science Instrumentation Centre (USIC), University of Delhi for providing scientific support and characterisation facilities for carrying out this research work.

References

1 E. Denkhaus and K. Salnikow, *Crit. Rev. Oncol. Hematol.*, 2002, **42**, 35–56.
2 K. S. Kasprzak, W. Bal and A. A. Karaczyn, *J. Environ. Monit.*, 2003, **5**, 183–187.
3 L. Feng, Y. Zhang, L. Wen, L. Chen, Z. Shen and Y. Guan, *Analyst*, 2011, **136**, 4197–4203.
4 V. K. Gupta, R. N. Goyal, S. Agarwal, P. Kumar and N. Bachheti, *Talanta*, 2007, **71**, 795–800.
5 Z. Sun, P. Liang, Q. Ding and J. Cao, *J. Hazard. Mater.*, 2006, **137**, 943–946.
6 A. M. Bond and G. G. Wallace, *Anal. Chem.*, 1983, **55**, 718–723.
7 M. K. Amini, T. Momeni-Isfahani, J. H. Khorasani and M. Pourhossein, *Talanta*, 2004, **63**, 713–720.
8 F. Wang, J. H. Moon, R. Nandhakumar, B. Kang, D. Kim, K. M. Kim, J. Y. Lee and J. Yoon, *Chem. Commun.*, 2013, **49**, 7228–7230.
9 K. Velmurugan, A. Raman, D. Don, L. Tang, S. Easwaramoorthi and R. Nandhakumar, *RSC Adv.*, 2015, **5**, 44463–44469.
10 W.-D. Li, Y. Huang, S.-Z. Li and W.-K. Dong, *J. Mol. Struct.*, 2023, **1284**, 135360.
11 L.-L. Man, L. Tong, L.-L. Gan, R.-Y. Li, H.-R. Mu and W.-K. Dong, *Phosphorus, Sulfur Silicon Relat. Elem.*, 2022, **197**, 1263–1272.
12 L.-L. Man, S.-Z. Li, J. Zhang, Y. Zhang and W.-K. Dong, *J. Photochem. Photobiol., A*, 2023, **437**, 114433.
13 I. Grabchev, J.-M. Chovelon and X. Qian, *New J. Chem.*, 2003, **27**, 337–340.
14 V. K. Gupta, A. K. Singh, L. K. Kumawat and N. Mergu, *Sens. Actuators, B*, 2016, **222**, 468–482.
15 D. Peralta-Domínguez, M. Rodríguez, G. Ramos-Ortíz, J. L. Maldonado, M. A. Meneses-Nava, O. Barbosa-García, R. Santillan and N. Farfán, *Sens. Actuators, B*, 2015, **207**, 511–517.
16 S. Goswami, S. Chakraborty, S. Paul, S. Halder and A. C. Maity, *Tetrahedron Lett.*, 2013, **54**, 5075–5077.
17 J. Jiang, C. Gou, J. Luo, C. Yi and X. Liu, *Inorg. Chem. Commun.*, 2012, **15**, 12–15.
18 H. Li, S.-J. Zhang, C.-L. Gong, Y.-F. Li, Y. Liang, Z.-G. Qi and S. Chen, *Analyst*, 2013, **138**, 7090–7093.
19 D. Udhayakumari and V. Inbaraj, *J. Fluoresc.*, 2020, **30**, 1203–1223.
20 A. Kumar, S. Mondal, K. S. Kayshap, S. K. Hira, P. P. Manna, W. Dehaen and S. Dey, *New J. Chem.*, 2018, **42**, 10983–10988.
21 R. Kumar, H. Jain, P. Gahlyan, A. Joshi and C. N. Ramachandran, *New J. Chem.*, 2018, **42**, 8567–8576.
22 Y. Zhou, J. F. Zhang and J. Yoon, *Chem. Rev.*, 2014, **114**, 5511–5571.
23 A. Gupta, S. Garg and H. Singh, *Anal. Methods*, 2020, **12**, 5022–5045.
24 Y. Li, X. Dong, C. Zhong, Z. Liu and J. Qin, *Sens. Actuators, B*, 2013, **183**, 124–128.
25 H. J. Kim, J. H. Lee and J.-I. Hong, *Tetrahedron Lett.*, 2011, **52**, 4944–4946.
26 S. K. Kim, D. H. Lee, J.-I. Hong and J. Yoon, *Acc. Chem. Res.*, 2009, **42**, 23–31.
27 A. Gogoi, S. Mukherjee, A. Ramesh and G. Das, *RSC Adv.*, 2015, **5**, 63634–63640.
28 S. Xu, M. He, H. Yu, X. Cai, X. Tan, B. Lu and B. Shu, *Anal. Biochem.*, 2001, **299**, 188–193.
29 H. N. Lee, K. M. K. Swamy, S. K. Kim, J.-Y. Kwon, Y. Kim, S.-J. Kim, Y. J. Yoon and J. Yoon, *Org. Lett.*, 2007, **9**, 243–246.
30 X. Meng, D. Cao, Z. Hu, X. Han, Z. Li, D. Liang and W. Ma, *Tetrahedron Lett.*, 2018, **59**, 4299–4304.
31 J. Zhang, M. She, J. Li, C. Wang, S. Wang, P. Liu, S. Zhang and J. Li, *Sens. Actuators, B*, 2018, **270**, 362–370.
32 Z. M. Dong, W. Wang, L. Y. Qin, J. Feng, J. N. Wang and Y. Wang, *J. Photochem. Photobiol., A*, 2017, **335**, 1–9.
33 S. Goswami, A. Manna, S. Paul, K. Aich, A. K. Das and S. Chakraborty, *Dalton Trans.*, 2013, **42**, 8078–8085.
34 W. Wang, J. Wei, H. Liu, Q. Liu and Y. Gao, *Tetrahedron Lett.*, 2017, **58**, 1025–1029.
35 W. Wang, M. Wu, H. Liu, Q. Liu, Y. Gao and B. Zhao, *Tetrahedron Lett.*, 2019, **60**, 1631–1635.
36 R. Bawa, N. Deswal, S. Negi, M. Dalela, A. Kumar and R. Kumar, *RSC Adv.*, 2022, **12**, 11942–11952.
37 R. Kumar, R. Bawa, P. Gahlyan, M. Dalela, K. Jindal, P. K. Jha, M. Tomar and V. Gupta, *Dyes Pigm.*, 2019, **161**, 162–171.
38 A. Kumar, B. Mohan, K. Modi, M. A. U. Din and S. Kumar, *J. Mol. Struct.*, 2022, **1268**, 133609.
39 Y. Xing, Z. Liu, Y. Xu, H. Wang, L. Li, B. Li, X. Yang, M. Pei and G. Zhang, *New J. Chem.*, 2020, **44**, 13875–13881.
40 H. Jain, N. Deswal, A. Joshi, C. N. Ramachandran and R. Kumar, *Anal. Methods*, 2019, **11**, 3230–3243.